J|A|C|S
ARTICLES
Published on Web 08/19/2006

Micelle Density Regulated by a Reversible Switch of Protein Secondary Structure

Rory E. Sallach,[†] Min Wei,[‡] Nilanjana Biswas,[§] Vincent P. Conticello,[||] Sébastien Lecommandoux,[⊥] Richard A. Dluhy,[§] and Elliot L. Chaikof*[,†,‡,#]

Contribution from the Department of Biomedical Engineering, Georgia Institute of Technology, Atlanta, Georgia 30332, Departments of Surgery and Biomedical Engineering, Emory University School of Medicine, Department of Chemistry, University of Georgia, Athens, Georgia, Department of Chemistry, Emory University, Atlanta, Georgia 30322, CNRS Laboratory of Organic Polymer Chemistry, University Bordeaux, 1 Talence Cedex, France, and School of Chemical and Biomolecular Engineering, Georgia Institute of Technology, Atlanta, Georgia 30332

Received June 1, 2006; E-mail: echaiko@emory.edu

Abstract: Protein secondary structures may exhibit reversible transitions that occur in an abrupt and controllable manner. In this report, we demonstrate that such transitions may be utilized in the design of a "smart" protein micellar system, in which a stimulus-induced change in protein structure triggers a rapid change in micelle compacticity and size. Specifically, recombinant DNA methods were used to prepare a protein triblock copolymer containing a central hydrophilic block and two hydrophobic end blocks derived from elastin-mimetic peptide sequences. Below the copolymer inverse transition temperature (T_t), dilute solutions of this amphiphilic protein formed monodispersed micelles in a narrow range of R_H of ~100 nm. When the the temperature was raised above T_t, an abrupt increase in micelle internal density was observed with a concomitant reduction in micelle size. This reversible change in micelle compacticity was triggered by helix-to-sheet protein folding transition. Significantly, these protein polymer-based micelles, which are rapidly responsive to environmental stimuli, establish a new mechanism for the design of controlled drug delivery vehicles.

Introduction

Designing peptide sequences that undergo conformational interconversions, such as helix−sheet switching, has been pursued through sequence manipulation of natural proteins and de novo sequence design.[1−3] These peptides have been used to elucidate complex folding mechanisms and have led to the suggestion that peptides that exhibit controlled structural plasticity may lead to the design of nanoscale devices, such as molecular switches or novel biomaterials.[4−6] Practical applications of peptides that display helix−sheet interconversion, however, have yet to be proven feasible because of slow structural transitions (minutes to hours), limited reversibility, and/or the severity of the initiating stimulus (e.g. prolonged exposure to high temperature or extremes in pH).

Elastin-mimetic proteins consisting of poly(VPGVG) or shorter peptides with the same repeat motif have been investigated by Raman and IR spectroscopy,[7] CD,[8,9] NMR,[10] X-ray diffraction,[11] and molecular dynamics simulations.[12] These studies reveal the formation of repetitive β-turn structures around Pro-Gly pairs, supporting a model in which the polypeptide forms a β-spiral structure.[13,14] Recent investigations, however, have demonstrated that the β-spiral likely represents only a *subset* of VPGVG-based elastic proteins. Specifically, solid state NMR analysis of an isotopically labeled model peptide $(VPGVG)_3$ has confirmed the presence of two types of minimum-energy conformers − one consisting of type II β-turns and the other comprised of *distorted* β-strand conformations.[15] The type II β-turn and distorted β-strand conformations have been previ-

[†] Department of Biomedical Engineering, Georgia Institute of Technology.
[‡] Emory University School of Medicine.
[§] University of Georgia.
[||] Emory University.
[⊥] University Bordeaux.
[#] School of Chemical and Biomolecular Engineering, Georgia Institute of Technology.

(1) Micklatcher, C.; Chmielewski, J. *Curr. Opin. Chem. Biol.* **1999**, *3*, 724−729.
(2) Gross, M. *Curr. Protein Pept. Sci.* **2000**, *1*, 339−347.
(3) Zhao, H.; Chen, M. H.; Shen, Z. M.; Kahn, P. C.; Lipke, P. N. *Protein Sci.* **2001**, *10*, 1113−1123.
(4) Takahashi, Y.; Ueno, A.; Mihara, H. *Structure* **2000**, *8*, 915−925.
(5) Zhang, S.; Rich, A. *Proc. Natl. Acad. Sci. U.S.A.* **1997**, *94*, 23−28.
(6) Ciani, B.; Hutchinson, E. G.; Sessions, R. B.; Woolfson, D. N. *J. Biol. Chem.* **2002**, *277*, 10150−10155.
(7) Prescott, B.; Renugopalakrishnan, V.; Thomas, G. J., Jr. *Biopolymers* **1987**, *26*, 934−936.
(8) Reiersen, H.; Clarke, A. R.; Rees, A. R. *J. Mol. Biol.* **1998**, *283*, 255−264.
(9) Arad, O.; Goodman, M. *Biopolymers* **1990**, *29*, 1652−1668.
(10) Urry, D. W.; Chang, D. K.; Krishna, N. R.; Huang, D. H.; Trapane, T. L.; Prasad, K. U. *Biopolymers* **1989**, *28*, 819−833.
(11) Cook, W. J.; Einspahr, H.; Trapane, T. L.; Urry, D. W.; Bugg, C. E. *J. Am. Chem. Soc.* **1980,** *102*, 5502−5505.
(12) Li, B.; Alonso, D. O.; Daggett, V. *J. Mol. Biol.* **2001**, *305*, 581−592.
(13) Venkatachalam, C. M.; Urry, D. W. *Macromolecules* **1981**, *14*, 1225−1229.
(14) Urry, D. W. J *Protein Chem* **1988**, *7*, 1−34.
(15) Yao, X. L.; Hong, M. *J. Am. Chem. Soc.* **2004**, *126*, 4199−4210.

10.1021/ja0638509 CCC: $33.50

ously detected in other VPGVG-like peptides using X-ray crystallography and solution NMR. For example, the crystal structure of Boc-VPGVG indicates a β-sheet conformation,[16] while solution NMR detected a β-turn structure for Boc-VPGVG-OMe.[17] Thus, it is now evident that the VPGVG repeat sequence has an inherent preference for either a β-sheetlike structure or a β-spiral-like conformation. Indeed, similar structures have been recently noted in native elastin.

Optical spectroscopic methods, including Fourier transform infrared, near-infrared Fourier transform Raman, and circular dichroism (CD) suggest that the global secondary structure of native elastin consists of ~10% α-helices, ~35% β-strands and ~55% disordered conformations.[18,19] Results obtained with specific elastin polypeptide sequences encoded by exons 3, 7, and 30 show that these hydrophobic peptides partly assume a polyproline II (PPII) helix structure.[20] Of particular interest, Tamburro et al.[21] have demonstrated that the exon 30 peptide is characterized by the presence of both PPII helix and β-sheet conformations. Significantly, the ratio of these structures depends on temperature, concentration, and time, with the PPII structure favored at low temperature and at low concentration and the β-sheet conformation preferred by opposite conditions.[22] The ease of the structural conversion of a PPII helix to a β strand has been demonstrated for other proteins[23,24] with this transition favored by an increase in temperature.[25] All told, helix and sheetlike structures appear to exist in native elastin and in structurally related peptides and proteins. Moreover, structural interconversions between these two conformations may be driven by an external stimulus, even in the absence of coacervation.

In this report, we describe the synthesis of a recombinant elastin-mimetic amphiphilic block copolymer and demonstrate that the interconversion of helix-sheetlike structures can be exploited to design a stimuli-responsive protein micellar system. Significantly, a temperature-induced change in protein secondary structure triggers a rapid, reversible, and discrete change in micelle compacticity.

Results and Discussion

We have recently developed a modular convergent biosynthetic strategy that has facilitated the synthesis of high-molecular weight recombinant protein block copolymers with significant flexibility in the selection and assembly of blocks of diverse size and structure.[26,29] This has led to the synthesis of a new

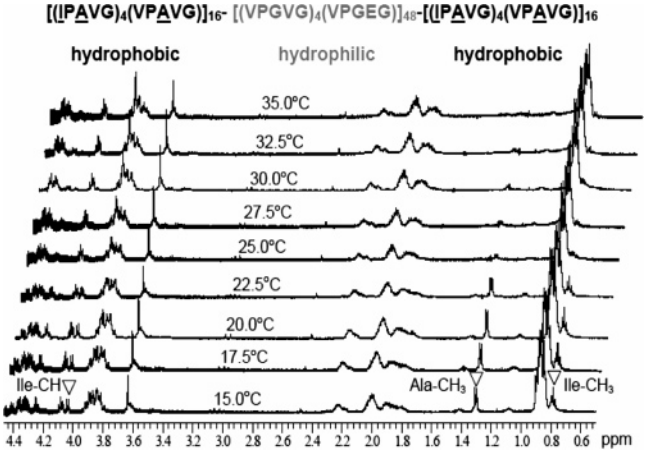

Figure 1. Temperature-dependent ^{1}H NMR spectra for 0.1% (w/v) protein triblock copolymer **B9** in D_2O.

Scheme 1. Amino Acid Sequence of Protein Triblock Polymer **B9** Derived from Concatemerization of Elastin Mimetic Peptide Sequences

[PN]-[X]-[PC]

PN = VPAVG[(IPAVG)$_4$(VPAVG)]$_{16}$IPAVG

X = VPGVG[(VPGVG)$_2$VPGEG(VPGVG)$_2$]$_{48}$VPGVG

PC = VPAVG[(IPAVG)$_4$(VPAVG)]$_{16}$IPAVG

class of BAB protein triblock copolymers that are derived from elastin-mimetic polypeptide sequences in which the respective blocks exhibit distinct structural features. In this investigation, a 165 kD amphiphilic polypeptide, designated **B9**, was expressed that incorporates identical endblocks of a hydrophobic sequence [(IPAVG)$_4$(VPAVG)]$_{16}$, separated by a central hydrophilic block [(VPGVG)4(VPGEG)]$_{48}$ (Scheme 1). The repeat sequences of this copolymer were designed such that the inverse temperature transition (T_t) of the endblocks would reside at or near 20 °C, while that of the central repeat unit would be significantly higher than 37 °C. Indeed, temperature-dependent ^{1}H NMR spectroscopy reveals that peaks assigned to alanine and isoleucine, which are uniquely present in the hydrophobic end block, disappear when an aqueous polymer solution is heated above 25 °C (Figure 1). In contrast, peaks characteristic of the hydrophilic midblock are unchanged, indicating that this portion of the triblock remains hydrated and molecularly mobile.

Fluorescence techniques have been widely used to probe the nanoscale structure of micelles. For example, pyrene is a polarity-sensitive compound in which a vibronic band at 373 nm undergoes significant intensity enhancement with increasing solvent polarity as compared to a band at 384 nm. Thus, the ratio of fluorescence emission intensities of these two vibronic bands (I_{373}/I_{384}) has been used to characterize the polarity of structured materials. Typically, a ratio of 1.15−1.20 indicates the formation micelles that contain a hydrophobic core and a hydrophilic corona.[32] In a 0.1% (w/v) solution of protein

(16) Ayato, H.; Tanaka, I.; Ashida, T. *J. Am. Chem. Soc.* **1981**, *103*, 5902−5905.
(17) Urry, D. W.; Cunningham, W. D.; Ohnishi, T. *Biochemistry* **1974**, *13*, 609−616.
(18) Debelle, L.; Alix, A. J.; Jacob, M. P.; Huvenne, J. P.; Berjot, M.; Sombret, B.; Legrand, P. *J. Biol. Chem.* **1995**, *270*, 26099−26103.
(19) Debelle, L.; Alix, A. J.; Wei, S. M.; Jacob, M. P.; Huvenne, J. P.; Berjot, M.; Legrand, P. *Eur. J. Biochem.* **1998**, *258*, 533−539.
(20) Bochicchio, B.; Ait-Ali, A.; Tamburro, A. M.; Alix, A. J. *Biopolymers* **2004**, *73*, 484−493.
(21) Tamburro, A. M.; Pepe, A.; Bochicchio, B.; Quaglino, D.; Ronchetti, I. P. *J. Biol. Chem.* **2005**, *280*, 2682−2690.
(22) Bochicchio, B.; Tamburro, A. M. *Chirality* **2002**, *14*, 782−792.
(23) Conway, K. A.; Harper, J. D.; Lansbury, P. T., Jr. *Biochemistry* **2000**, *39*, 2552−2563.
(24) von Bergen, M.; Friedhoff, P.; Biernat, J.; Heberle, J.; Mandelkow, E. M.; Mandelkow, E. *Proc. Natl. Acad. Sci. U.S.A.* **2000**, *97*, 5129−5134.
(25) Shi, Z.; Olson, C. A.; Rose, G. D.; Baldwin, R. L.; Kallenbach, N. R. *Proc. Natl. Acad. Sci. U.S.A.* **2002**, *99*, 9190−9195.
(26) Wright, E. R.; McMillan, R. A.; Cooper, A.; Apkarian, R. P.; Conticello, V. P. *Adv. Funct. Mater.* **2002**, *12*, 149−154.
(27) Wright, E. R.; Conticello, V. P. *Adv. Drug Delivery Rev.* **2002**, *54*, 1057−1073.
(28) Daniell, H.; Guda, C.; McPherson, D. T.; Zhang, X.; Xu, J.; Urry, D. W. *Methods Mol. Biol.* **1997**, *63*, 359−371.
(29) Nagapudi, K.; Brinkman, W. T.; Leisen, J.; Thomas, B. S.; Wright, E. R.; Haller, C.; Wu, X.; Apkarian, R. P.; Conticello, V. P.; Chaikof, E. L. *Macromolecules* **2005**, *38*, 345−354.
(30) Faucher, K. M.; Dluhy, R. A. *Colloids Surf., A* **2003**, *219*, 125−145.
(31) Elmore, D. L.; Dluhy, R. A. *J Physi Chemistry B* **2001**, *105*, 11377−11386.
(32) Wilhelm, M.; Zhao, C. L.; Wang, Y. C.; Xu, R. L.; Winnik, M. A.; Mura, J. L.; Riess, G.; Croucher, M. D. *Macromolecules* **1991**, *24*, 1033−1040.

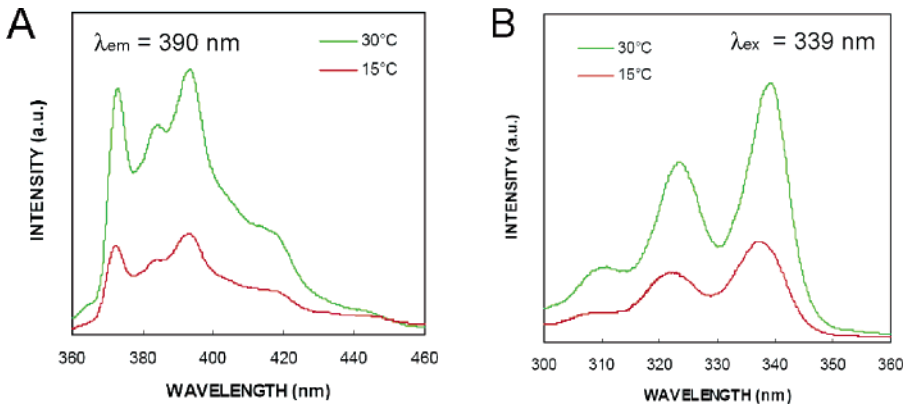

Figure 2. Fluorescence emission (A) and excitation (B) spectra of pyrene (6×10^{-7} M), monitored at 339 nm and 390 nm, respectively, for a 0.1% (w/v) protein solution at 15 and 30 °C.

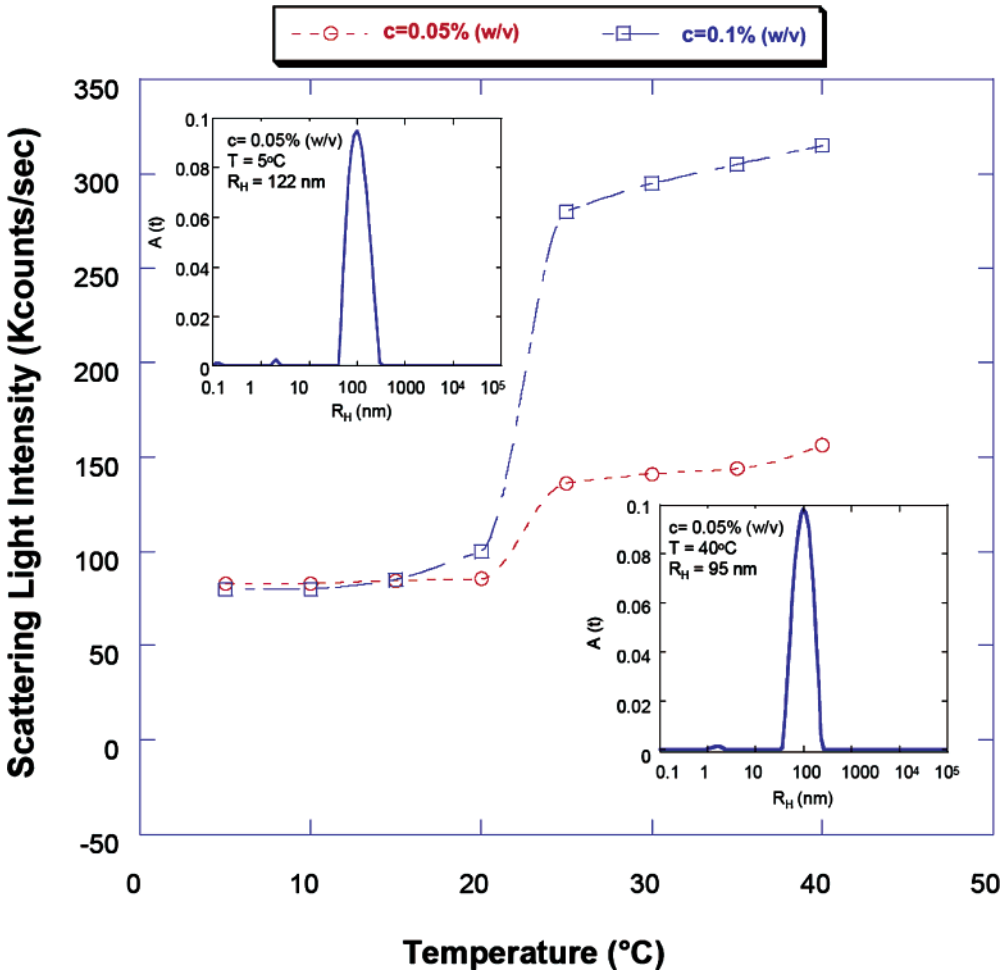

Figure 3. Scattering light intensity as a function of temperature for the samples with different concentrations (0.05% (w/v) and 0.1% (w/v). When the aqueous concentration is higher than 0.3% (w/v), the sample tends to form hydrogel, and scattering light intensity exceeds the detection maximum. Insets represent micelle size distribution at 15 and 30 °C (0.05 (w/v) in water). Temperature-varied dynamic light scattering was used to determine the mean micelle size and micelle size distributions.

copolymer, values for I_{373}/I_{384} were 1.178 at 15 °C and 1.172 at 30 °C. These values confirmed the presence of micellar structure at temperatures both above and below the T_t for the protein endblock. It was also noteworthy that the intensity ratios of I_{338}/I_{332} in the pyrene excitation spectra were 1.548 for 15 °C and 2.149 for 30 °C, which demonstrate an increase in pyrene partitioning to an apolar environment above T_t. Consistent with these observations, a substantial increase in both emission and excitation intensities was noted on increasing the solution temperature from 15 to 30 °C, which reflects substantial dehydration of the hydrophobic micelle core. Fluorescence emission and excitation spectra of pyrene (6×10^{-7}M), monitored at 339 nm and 390 nm, respectively, for a 0.1% (w/v) protein solution at 15 and 30 °C are presented in Figure 2.

Dynamic light scattering was used to examine in detail the micellization process, as well as micelle structure and size distribution using a Laplace inversion algorithm (Figure 3). These investigations were conducted from 5 to 40 °C, with light

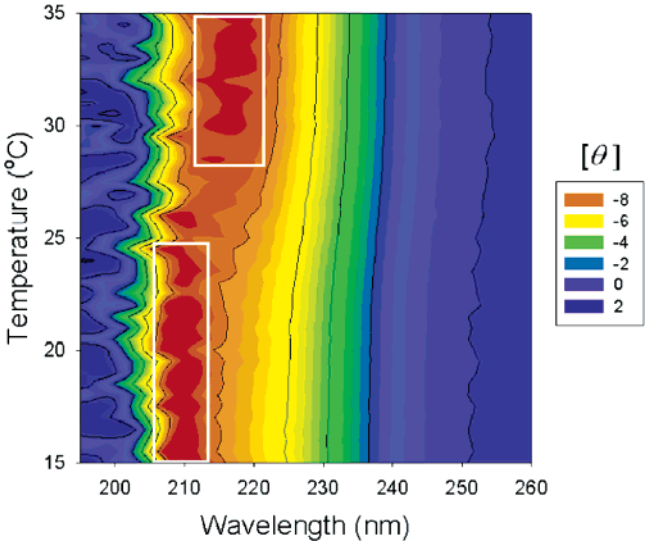

Figure 4. Circular dichroism spectra presented as a contour plot (molar ellipticity, θ, in 10^6 degrees cm^2 dmol^{-1}) of a 0.1% (w/v) protein.

scattering measured at angles between 40° to 150°. At low temperature, average R_H ranged from 104 to 122 nm. Of note, the linearity of the plot of frequency Γ versus q^2 attests to the spherical shape of the micelles (see Supporting Information). At temperatures exceeding 25 °C, a large increase in scattering intensity was observed, which was accentuated in micelles formed in solutions of higher protein concentration. Calculations of R_H revealed a decrease in micelle size above the transition temperature consistent with the formation of denser structures. This corroborates the previous observations by fluorescence spectroscopy in which the environment of pyrene is more hydrophobic. That is, at low temperature, protein micelles likely consist of a core−shell morphology with a relatively loose water-filled core, but micelles are dehydrated and compacted at high temperatures. The low light-scattering intensities observed at low temperature suggest that the micelles are highly hydrated and thus have low scattering contrast. Increasing protein concentration appears to amplify the effect on micelle compacticity and, as such, is associated with an increase in light-scattering intensity at high temperature. It is also noteworthy that the transition between these two largely monodispersed micelle populations was both rapid and reversible over multiple heating and cooling cycles.

Circular dichroism (CD) spectroscopy was used to examine protein conformation over a temperature range of 15−35 °C (Figure 4). The spectra demonstrated a secondary structure transition, which begins at 24 °C and is complete at 27 °C, reflected in a shift of a negative peak from 208 to 216 nm, characteristic of a helix-to-sheet transition. CD curves over multiple heating and cooling cycles confirmed that this transition was reversible. Circular dichroism spectra of 0.1% (w/v) protein polymer aqueous solution at 15 and 30 °C upon heating and cooling are presented in Figure 5.

The amide I and II regions in the ATR spectra of a 10% aqueous solution of **B9** collected between −10 and 65 °C are shown in Figure 6. Below ∼20 °C the most predominant intensity in the broad amide I band appears at 1654 cm^{-1}, corresponding to an α-helical component. However, the broadness of the amide I band (full width at half-height ∼65 cm^{-1}) is indicative of the presence of various conformers. With

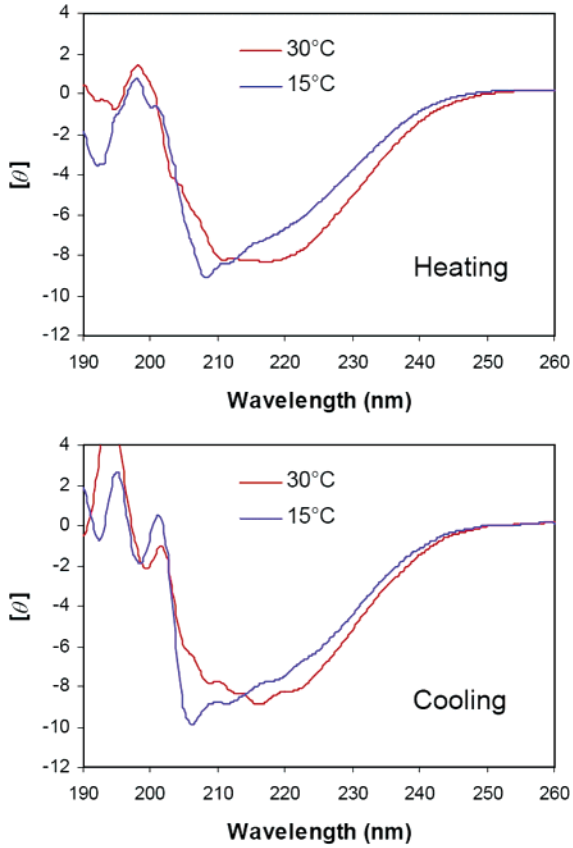

Figure 5. Circular dichroism (CD) spectra (molar ellipticity, θ, in 10^6 degrees cm^2 dmol^{-1}) of 0.1%(w/v) protein/polymer aqueous solution at 15 and 30 °C upon heating and cooling.

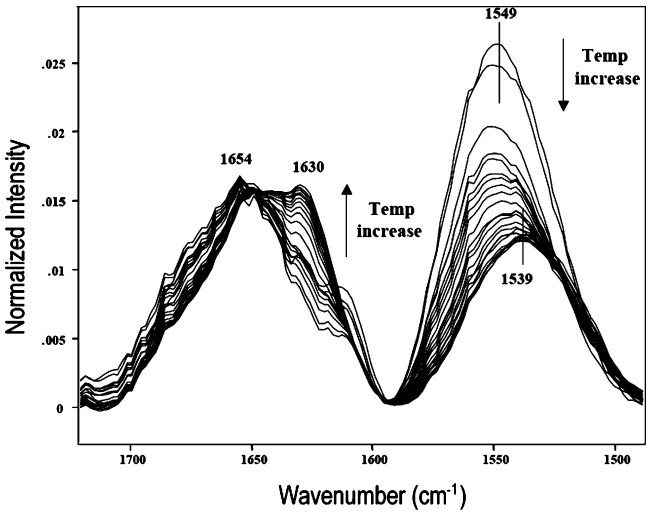

Figure 6. ATR IR spectra of a 10% **B9** solution in water as a function of temperature between 2 and 60 °C. The 1630 cm^{-1} becomes more prominent from ∼17 °C. The amide II peak appears at 1549 cm^{-1} from −10 to ∼17 °C, after which it gradually shifts to ∼1539 cm^{-1}.

increasing temperature, a β-sheet component at 1630 cm^{-1} becomes more prominent, although the intensity of the α-helix band does not change appreciably. Figure 7 illustrates the variation with temperature of the ratio of band intensity of 1630 cm^{-1} to 1654 cm^{-1} peaks (I_{1630}/I_{1654}). The anomalous behavior of the curve in the temperature range of −4 to 0 °C is likely due to the phase transition of water from the solid to the liquid state.

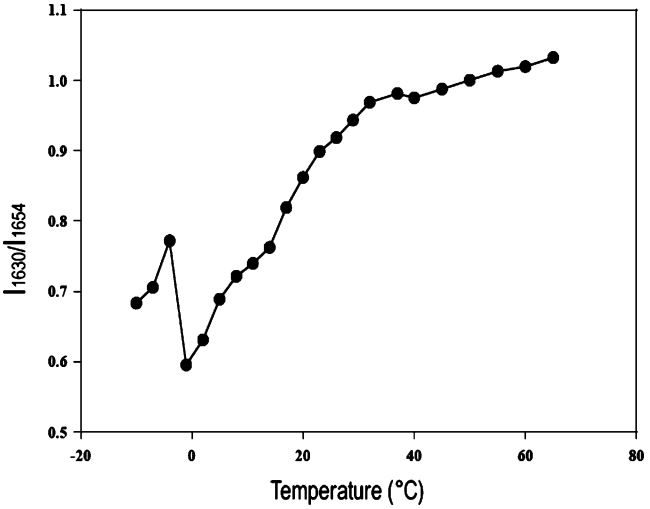

Figure 7. Ratio of absorbance bands at 1630 to 1654 cm^{-1} as a function of temperature between −10 and 60 °C in water.

The increase in prominence of the β-sheet component is also accompanied by a band shift in the amide II region. The peak maximum of the amide II band shifts by approximately 10 wavenumbers from 1549 to 1539 cm^{-1}. The amide II band intensity also decreases relative to that of the amide I region with increasing temperature (Figure 6).

We have used the mathematical technique of two-dimensional correlation spectroscopy[33] to further analyze the temperature-dependent ATR-IR spectra. In particular, the $\beta\nu$ two-dimensional correlation technique[31,34] was used to provide increased resolution enhancement of the underlying bands in the amide I contour, as well as to determine the temporal order of events produced by changes in the local molecular environment of **B9** upon sample heating. The $\beta\nu$ correlation method provides a more quantitative description of the degree of coherence between the observed spectral intensity changes and the sequence of molecular rearrangements in a discrete set of time-dependent spectra.[31,34] This method has previously been used to analyze the dynamic structural response of the amide I bands in proteins and peptides following sample perturbation.[35, 36]

The $\beta\nu$ plots for the amide I region of **B9** are presented in Figure 8, while the corresponding band assignments for the correlation peaks along with their effective phase angle values, β_e, are presented in Table 1. Figure 8 and Table 1 present the $\beta\nu$ correlation data for two subsets of the ATR spectra collected over the temperature range from 2 to 65 °C. The $\beta\nu$ plot for the low-temperature spectral subset (2−20 °C) shown in Figure 8A shows one major correlation peak at ∼1627 cm^{-1} and a minor peak at ∼1688 cm^{-1}. The wavenumber peaks 1627 and 1688 cm^{-1} correspond to β-sheet structures.[37] The β_e effective phase angle for the major β structure corresponding to the 1627 cm^{-1} peak is greater than the β_e value calculated for the 1688 cm^{-1} peak (285.2 vs 234.3), indicating that the former reorients at a faster rate than the latter.

Table 1. Effective Phase Angle Values, β_e, for a 10% **B9** Solution in the Amide I Region

β_e Values Taken from Figure 8A (2 to 20 °C)		
wavenumber (cm^{-1})	assignment	β_e
1627.0	β-sheet	285.2
1688.6	β-sheet/β-turn	234.3
β_e Values Taken from Figure 8B (20 to 65 °C)		
wavenumber (cm^{-1})	assignment	β_e
1629.3	β-sheet	285.2
1644.6	unordered	281.4
1650.7	α-helix	275.3
1681.7	β-turn	259.4
1693.7	β-sheet/β-turn	243.4

The $\beta\nu$ plot for the high-temperature spectral subset (20−65 °C) of the **B9** polymer indicates that significant spectral changes occur as the temperature increases (Figure 8B). Major correlation intensity is observed at wavenumber peak positions corresponding to α-helical structures (1650 cm^{-1}), β-sheet structures (1629, 1681, 1693 cm^{-1}), and unordered structures (1644 cm^{-1}). The β_e effective phase angle values for each of these structural units are grouped with a range (∼240−290) that indicates similar dynamic behavior for all the observed secondary structures.

The $\beta\nu$ plots of Figure 8 clearly show evidence for the temperature-dependent reorganization of the secondary structure of the **B9** polymer. At low temperatures (below 20 °C), the predominate structural response of **B9** to increasing temperature is the formation and rearrangement of β-sheet structures. Above 20 °C, all the **B9** conformations, i.e., helix, sheet, and unordered, are coherently correlated. All told, IR spectroscopy is consistent with a helix-to-sheet transition upon increasing temperature. Specifically, while there is a predominance of helix structures below 20 °C, as the temperature rises, the molecular reorganization of β-sheet structures is preferred relative to all other secondary structures. In contrast, a dynamic equilibrium exists above 20 °C among all coexisting secondary structures.

Since NMR spectroscopy demonstrated collapse of the protein endblocks over this thermal transition, we believe that the interconversion between helix and sheetlike structures revealed by CD and IR spectroscopy likely arises within the micelle core, where an increase in hydrophobicity is known to favor sheet conformation.[38] Significantly, assemblies of β-sheet peptides are more compact than those of α-helices, consistent with an increase in micelle density and reduction in size.[39] The induction of a change in micelle density and size by a thermally triggered protein folding transition is illustrated in Scheme 2. Admittedly, given the triblock structure of the protein polymer, it is possible that the micelles consist of a more heterogeneous microgel-like or "tapioca" structure rather than a classic "core−shell" system. In this regard, we have previously demonstrated that micellar nanoparticles displaying a core−corona structure can be generated from an amphiphilic elastin-mimetic protein/diblock polymer.[40] At temperatures below the phase transition of the hydrophobic block, the solution consisted of isolated

(33) Noda, I.; Ozaki, Y. *Two-Dimensional Correlation Spectroscopy: Applications in Vibrational and Optical Spectroscopy*; J. Wiley & Sons: Chichester, 2004; p 290.
(34) Shanmukh, S.; Dluhy, R. A. *J. Phys. Chem. A* **2004**, *108*, 5625−5634.
(35) Shanmukh, S.; Howell, P.; Baatz, J.; Dluhy, R. *Biophys. J.* **2002**, *83*, 2126−2141.
(36) Shanmukh, S.; Biswas, N.; Waring, A. J.; Walther, F. J.; Wang, Z.; Chang, Y.; Notter, R. H.; Dluhy, R. A. *Biophys. Chem.* **2005**, *113*, 233−244.
(37) Goormaghtigh, E.; Cabiaux, V.; Ruysschaert, J. Determination of soluble and membrane protein structure by Fourier transform infrared spectroscopy. I. Assignments and model compounds. In *Physiochemical Methods in the Study of Biomembranes*; Hilderson, H., Ralston, G., Eds.; Plenum Press: New York, 1994; pp 329−362.
(38) Carrier, D.; Mantsch, H. H.; Wong, P. T. T. *Biopolymer* **1990**, *29*, 837−844.
(39) Chalikian, T. V. *Annu. Rev. Biophys. Biomol. Struct.* **2003**, *32*, 207−235.
(40) Lee, T. A. T.; Cooer, A.; Apkarian, R. P.; Conticello, V. P. *Adv. Mater.* **2000**, *12*, 1105−1110.

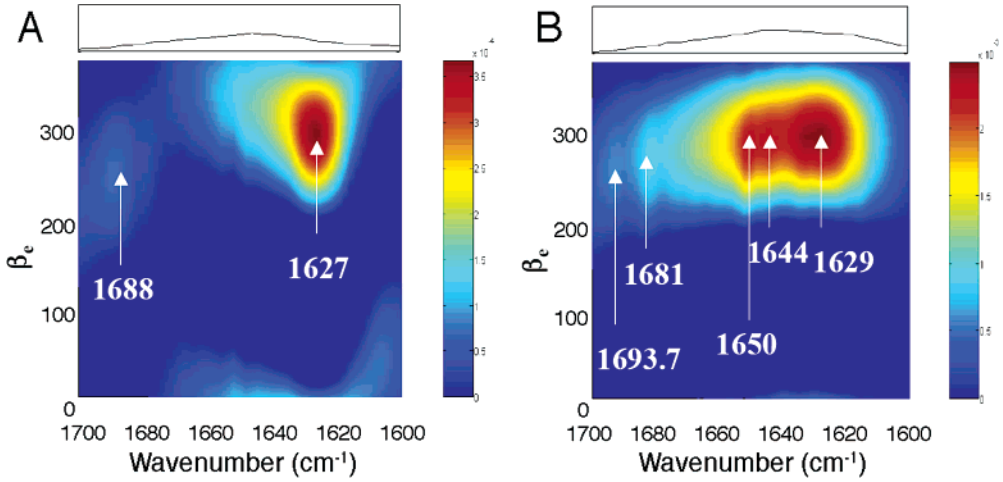

Figure 8. $\beta\nu$ Correlation plots from the ATR spectra of 10% **B9** solution in the amide I region from (A) 2 to 20 °C and (B) 20 to 65 °C.

Scheme 2. Temperature-Mediated Helix-Sheet Interconversion Provides a Molecular Trigger that Regulates Micelle Internal Density and Size

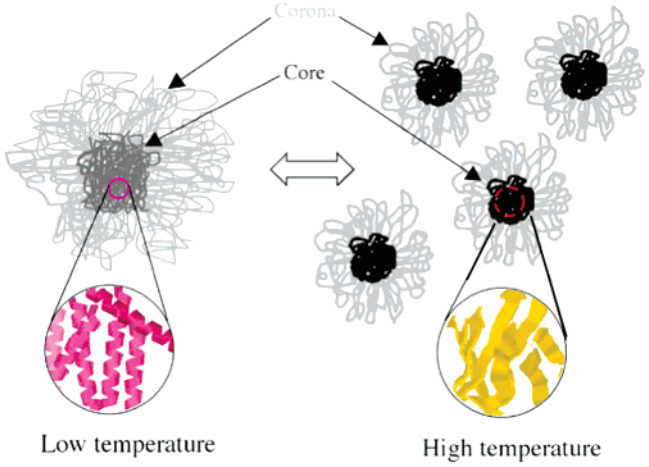

peptide chains that self-assemble as micelles above the transition temperature. The current investigation demonstrates that amphiphilic proteins can form micellar nanoparticles below the transition temperature when tailored to express a sufficiently large hydrophobic component. Significantly, as a consequence of altering block design, a temperature-induced helix-to-sheet structural transition provides a unique mechanism for reversibly controlling additional particle features, such as internal compacticity and size.

Conclusion

A stimuli-responsive protein micelle system is presented that relies upon a reversible switch of secondary structure. Below a transition temperature, dilute solutions of this amphiphilic protein form monodispersed micelles with a relatively loose and hydrated internal structure. Upon raising the temperature, we observed an abrupt increase in micelle compacticity with a reduction in particle size. This reversible change in micelle structure is triggered by a thermally induced helix-to-sheet protein folding transition, where the activating temperature is tunable through alterations in the peptide sequence. Given the potential of protein systems to provide a biocompatible and biodegradable vehicle for drug or compound delivery, we anticipate these temperature-responsive micelles will find application in a variety of biomedical and nonmedical technologies. For example, it is possible to envision the use of stimuli responsive micelles to tune drug release rates for optimized targeted drug delivery systems for both pharmacological, nutriceutical, and cosmetic applications. Moreover, by conjugating these proteins to gold or metal nanocrystals, local thermal changes could be induced by remote application of a radio frequency magnetic field, which may facilitate site-targeted therapies. Alternatively, this system could find application as nanoscale reactors for the optimization of local stimuli-responsive reaction conditions.

Acknowledgment. This work was supported by NIH grants EB001956 (R.A.D.), HL60464 (E.L.C. and V.P.C.), and HL71336 (E.L.C. and V.P.C.). We thank Prof. L. Andrew Lyon, Mr. Satish Nayak, and Mr. Nicolas Guidolin for helpful discussion and assistance with DLS studies.

Supporting Information Available: Detailed Experimental Section and DLS analysis. This material is available free of charge via the Internet at http://pubs.acs.org.

JA0638509